Experimental comparison of extreme-ultraviolet multilayers for solar physics

David L. Windt, Soizik Donguy, John Seely, and Benjawan Kjornrattanawanich

We compare the reflectance and stability of multilayers comprising either Si/Mo, Si/Mo_2C, Si/B_4C, Si/C, or Si/SiC bilayers, designed for use as extreme-ultraviolet (EUV) reflective coatings. The films were deposited by using magnetron sputtering and characterized by both x-ray and EUV reflectometry. We find that the new Si/SiC multilayer offers the greatest spectral selectivity at the longer wavelengths, as well as the greatest thermal stability. We also describe the optimization of multilayers designed for the Solar-B EIS instrument. Finally, we compare experimental reflectance data with calculations and conclude that currently available optical constants cannot be used to adequately model the performance of many of these multilayers.

OCIS Codes: 230.4170, 310.1620, 310.6860, 340.0340, 350.1260.

1. Introduction

Periodic multilayer films have been developed in recent years for use as reflective coatings operating at normal incidence in the soft-x-ray and extreme-ultraviolet (EUV) spectral regions. The coatings comprise a stack of nanometer-scale bilayers of optically dissimilar materials, arranged so that the reflections occurring at each interface in the stack achieve constructive interference over a range of photon wavelengths and incidence angles. The response of the coating can be tuned in wavelength λ by adjusting the multilayer period d (i.e., the bilayer thickness), according to Bragg's law $n\lambda = 2\,d\,\cos\theta$ (with an appropriate correction for refraction), where θ is the incidence angle and n is the Bragg order (which is generally set equal to 1 for normal incidence multilayers.) The number of bilayers and the relative thickness of each constituent material can also be adjusted in order to control to some extent the spectral response of the coating.

Multilayer structures that contain Si in particular, a material that has relatively low absorption at wavelengths longer than the Si L absorption edge ($\lambda \sim 12.4$ nm), have found broad application in the EUV in a variety of scientific and technological disciplines, including solar physics, plasma physics, and photolithography. The Si/Mo multilayer system is perhaps the best studied,[1,2,3] owing largely to its important application in photolithography. Other Si-based EUV multilayers that have been investigated previously include Si/Mo_2C, Si/B_4C, and Si/C.[4,5]

In this work we focus primarily on the performance of EUV multilayers for use in solar physics, specifically in high-angular-resolution or high-spectral-resolution instruments employing normal-incidence mirrors and gratings. The EUV solar spectrum is rich with line emission from a variety of ions present in the solar corona and transition region, formed at plasma temperatures of up to several million degrees.[6,7,8] Quasi-monochromatic (or quasi-isothermal) images of the corona or transition region thus can be obtained by using normal-incidence telescopes coated with narrow-band multilayers tuned to specific emission lines. This approach was employed in both the SOHO EIT[9] and TRACE[10] satellite instruments, which used Si/Mo and Si/Mo_2C multilayers, respectively, and will be used in future solar missions as well, such as the SDO AIA, Solar Orbitor, RAM, and others. The degree to which such high-resolution images can be used to unambiguously unravel the plasma morphology and dynamics depends, however, on their spectral purity.[11] That is, although a multilayer coating can be tuned precisely so that the peak reflectance is matched to a particular wavelength corresponding to emission from a specific ion, in the EUV the spectral bandpass of the

D. L. Windt (windt@astro.columbia.edu) and S. Donguy are with the Columbia Astrophysics Laboratory, 550 West 120th Street, New York, New York 10027. J. Seely is with the Naval Research Laboratory, 4555 Overlook Avenue, S.W., Washington, D.C. 20375. B. Kjornrattanawanich is with the Universities Space Research Association, National Synchrotron Light Source, Beamline X24C, Brookhaven National Laboratory, Upton, New York 11973.

Received 26 June 2003; accepted 14 November 2003.
0003-6935/04/091835-14$15.00/0

coating is generally wide enough to include at least some spectral contamination from adjacent wavelengths due to emission from ions formed at other plasma temperatures. (This is of particular concern especially in the vicinity of the bright He II line at 30.4 nm.) Future solar imaging missions therefore will benefit greatly from new multilayers having a more narrow spectral response in order to reduce such spectral contamination.

Another powerful observational technique, complementary to the narrowband high-resolution imaging approach just outlined, is to employ broadband multilayer-coated normal-incidence optics for the construction of high-resolution EUV spectrometers. This approach, as will be used for example in the Solar-B EIS instrument currently under development, can be used to measure spectroscopic line profiles in order to elucidate the physics underlying the formation and evolution of the complex elementary structures observed in the dynamic Sun. In this case, multilayers having a broad spectral response are required in order to maximize the efficiency of the spectrometer over a wide range of wavelengths.

Here we describe research directed therefore at the development of two classes of EUV multilayers optimized for solar instrumentation. The first class is designed specifically for narrowband operation in the wavelength range $\lambda \sim 25$–35 nm. This portion of the EUV is of particular interest for the development of future solar imagers (where the performance of traditional Si/Mo multilayers is less than optimal), as it includes diagnostically important coronal and transition-region emission lines from Fe XV (28.4 nm), He II (30.4 nm), and Fe XVI (33.5 nm). The second class of multilayers we describe is designed for broadband operation in the range $\lambda \sim 18$–30 nm; the research presented here on this topic was specifically directed at the development of multilayers for use in the Solar-B EIS instrument,[12] which employs a parabolic focusing mirror and a toroidal grating, both operating at normal incidence. In the EIS instrument, each half of each optical element is coated with a broadband multilayer; one channel is tuned to operate from $\lambda \sim 18$ to $\lambda \sim 21$ nm, the other is tuned for $\lambda \sim 25$ to $\lambda \sim 29$ nm.

We have fabricated by magnetron sputtering a variety of prototype multilayers containing Si/Mo, Si/Mo_2C, Si/B_4C, and Si/C bilayers, as well as new multilayer system containing Si/SiC bilayers. Structural characterization was performed by using grazing-incidence x-ray reflectometry (XRR) by using Cu K-α radiation, and the EUV performance was determined from normal-incidence reflectometry. We have explored the stability to heat and oxidation by characterizing films before and after thermal anneals in air. In the case of the Si/Mo and Si/Mo_2C systems we have also studied the effectiveness of thin Si capping layers intended to mitigate oxidation (since in these systems it is sometimes desirable to use Mo as the topmost layer in the multilayer stack to maximize the reflectance) and have optimized the response of these films by varying precisely the fractional Si-layer thickness. We have attempted to fit the measured EUV reflectance curves in all cases by using available optical constants, and we have compared the structural parameters determined from XRR with those used to fit the EUV data. To better fit the Si/Mo_2C reflectance data in particular, we have also generated new EUV optical constants for Mo_2C, using the reflectance-versus-incidence-angle technique.

Table 1. Effective Deposition Rates[a]

Material	Power (W)	Rate (nm/s)
Si	600	0.40
Mo	400	0.56
Mo_2C	400	0.36
B_4C	500	0.05
C	1000	0.10
SiC	500	0.14

[a]Prepared by dc magnetron sputtering in Ar at the specified cathode powers.

The remainder of this paper is organized as follows. In Section 2 we describe the experimental techniques used for film growth and characterization. We present and discuss the experimental results just outlined in Section 3. Finally, in Section 4 we summarize our findings and outline some prospects for the future.

2. Experimental Procedures

The multilayer films discussed here were prepared by dc magnetron sputtering with a deposition system that has been described previously.[13] Films were deposited onto polished Si (100) wafer segments measuring 1 cm $\times$ 1 cm. The background pressure in the vacuum chamber prior to deposition was less than 1×10^{-6} Torr in all cases (except where noted below), and the sputter gas (Ar) pressure was maintained at 1.50 ± 0.01 mTorr during growth. Individual layer thicknesses were controlled by varying the computer-controlled rotation rate, and hence the exposure time, of the substrate as it passed over each magnetron cathode. The effective deposition rates listed in Table 1 were computed by using layer thicknesses determined from XRR measurements (described below) divided by the known exposure times.

XRR measurements were made in the θ-2θ geometry by using of a four-circle x-ray diffractometer having a sealed-tube Cu source and a Ge (111) crystal monochromator tuned to the Cu K-α line ($\lambda = 0.154$ nm, $E = 8.04$ keV.) The angular resolution of this system is estimated to be $\delta\theta \sim 0.015°$. Fits to the XRR data (performed by using IMD[14]) were used to determine the multilayer period, with an estimated precision of $\delta d \sim \pm 0.01$ nm; from the relative heights of the Bragg peaks, the fractional Si-layer thickness $\Gamma_{Si} = d_{Si}/d$, with an estimated precision of $\delta\Gamma \sim \pm 0.025$; we can also deduce from these fits the average interface widths, σ, with a precision of $\delta\sigma \sim \pm 0.05$ nm.

EUV reflectance measurements were made near normal incidence (4°) with a laser-plasma-based reflectometer at Columbia University, also described

Table 2. Structural Parameters Determined from XRR and EUV Reflectance Measurements and EUV Performance Characteristics[a]

		XRR			EUV						
Materials	N	d (nm)	Γ_{Si}	σ (nm)	d (nm)	Γ_{Si}	σ (nm)	R_{max} (%)	λ_{max} (nm)	FWHM (nm)	Rejection
Si/Mo	30	14.88	0.86	0.5	15.00	0.90	0.50	22.4	27.9	1.610	6.6× to 30.4 nm
		16.00	0.86	0.5	16.15	0.90	0.30	19.7	29.9	1.452	4.3× to 28.4 nm
		17.98	0.87	0.5	18.05	0.85	0.20	15.5	32.9	1.525	5.2× to 30.4 nm
Si/Mo_2C	30	14.73	0.89	0.4	14.88	0.90	1.23	19.0	27.8	1.390	9.6× to 30.4 nm
		15.95	0.89	0.4	16.15	0.89	1.50	15.8	29.8	1.398	4.9× to 28.4 nm
		17.73	0.89	0.4	17.93	0.90	1.80	13.1	32.7	1.447	6.2× to 30.4 nm
Si/B_4C	30	15.20	0.69	0.6	15.30	0.68	0.40	35.3	28.1	1.584	7.0× to 30.4 nm
		16.45	0.69	0.6	16.50	0.68	1.00	29.1	29.8	1.970	7.7× to 28.4 nm
		18.75	0.69	0.6	18.35	0.68	0.80	26.5	32.9	2.060	10.3× to 30.4 nm
Si/C	30	14.70	0.65	0.6	15.05	0.70	1.50	19.0	27.5	1.600	4.7× to 30.4 nm
		15.80	0.65	0.6	16.28	0.70	1.55	17.8	29.4	1.980	5.3× to 28.4 nm
		17.80	0.65	0.6	18.10	0.70	1.60	16.9	32.3	2.570	7.1× to 30.4 nm
Si/SiC	30	15.05	0.60	0.5	15.18	0.60	1.60	18.5	27.9	1.272	13.1× to 30.4 nm
		16.43	0.60	0.5	16.48	0.60	1.80	17.2	29.8	1.470	14.0× to 28.4 nm
		18.25	0.60	0.5	18.50	0.60	1.80	16.7	32.8	1.713	15.0× to 30.4 nm

[a]Shown in Figs. 1, 6(b), 7(b), and 9.

previously.[13] The reflectance of selected samples was also measured by using synchrotron radiation at 5° incidence, using the Naval Research Laboratory (NRL) reflectometer on beamline X24C at the National Synchrotron Light Source (NSLS), Brookhaven National Laboratory. The accuracy and wavelength scale of the NRL reflectometer has been verified by cross calibration of witness samples at the Calibration and Standards Beamline 6.3.2 at the Advanced Light Source (ALS).[15] The wavelength scale of the Columbia reflectometer was likewise calibrated; however, this reflectometer suffers from spectral contamination at the EUV wavelengths considered here at present (owing to higher-order reflections from the grating monochromator), and so the absolute reflectance values obtained with this system are ~5%–10% too low. Fits to the NSLS EUV data (also made by using IMD) were used to infer structural parameters, which we compare to those same parameters determined from XRR. However, as we discuss in detail in Subsection 3.C, the quality of the EUV fits, and thus the inferred structural parameters, is highly dependent on the accuracy of the optical constants used to compute the reflectance and on the precise condition of the film surface (e.g., thickness of any oxide layers.) Because of the considerable uncertainty associated with both of these factors, the reliability of the EUV-derived parameters is not high, in general.

3. Results and Discussion

A. Narrowband Multilayers

We summarize in Table 2 the results obtained for an array of Si/Mo, Si/Mo_2C, Si/B_4C, Si/C, and Si/SiC multilayers, all containing $N = 30$ bilayers, with periods ranging from d~14.7 to d~18.8 nm, designed for use near normal incidence at wavelengths λ in the range 28–34 nm. To achieve a relatively narrow spectral response, we adjusted the fractional Si-layer thickness Γ for each multilayer system on the basis of calculations using available optical constants (described in Subsection 3.C). For each of these multilayers, modeling indicated that using Si as the topmost layer in the multilayer stack results in lower reflectance relative to the other way around. However, in the case of the Si/Mo and Si/Mo_2C multilayers in particular the degradation in reflectance resulting from oxidation of these metal layers would be greater relative to the ease of using Si used as the topmost layer. (Si oxidizes as well, of course, but the sensitivity to oxidation is greater when the metal layers are on top because of the location, relative to the top surface of the film, of the antinodes in the standing waves formed during use). In order to mitigate oxidation of these metal layers, 2-nm-thick Si capping layers were used with these two multilayer systems, and we discuss in more detail in Subsection 3.B the effectiveness of this technique. (Because of their lower susceptibility to oxidation, no capping layers were required with multilayers by using B_4C, C, or SiC as the topmost layer.) Furthermore, a narrow spectral response requires relatively thin metal layers (~2 nm) for both of these systems, so the requisite Γ values are large: the actual values determined from XRR are $\Gamma = 0.86$ for Si/Mo and $\Gamma = 0.89$ for Si/Mo_2C. In contrast, because of their lower absorption at EUV wavelengths, multilayers containing B_4C, C, or SiC that achieve optimal narrowband spectral response require thinner Si layers and thus smaller Γ values, in the range 0.6–0.69 (i.e., comparable with the Γ values used in Si/Mo multilayers designed for high reflectance at shorter wavelengths, e.g., $\lambda = 13.4$ nm, as in EUV lithography.)

For each of the five multilayer systems considered, we prepared films intended to be tuned to the emission lines of Fe XV (28.4 nm), He II (30.4 nm), and Fe XVI (33.5 nm), i.e., fifteen samples total. The EUV reflectance results of using synchrotron radiation at NSLS, also listed in Table 2, revealed that the peak

wavelengths in all cases were systematically shorter than the target wavelengths, typically by $\delta\lambda \sim 1$ nm; schedule and resource limitations precluded the possibility of preparing new samples with slightly larger periods. However, the measured peak wavelengths are close enough to the target wavelengths, arguably, to warrant relative comparisons between the different multilayers and to justify the conclusions we draw below regarding the utility of these coatings for future solar instruments.

To facilitate such relative performance comparisons (particularly the spectral selectivities derived below), we show in Fig. 1 the measured normal-incidence reflectance curves of the samples listed in Table 2, where we have slightly adjusted the wavelength scale for each sample independently in these plots so that the peak wavelengths overlap. The highest peak reflectance by far at all wavelengths is obtained with the Si/B_4C multilayer system, which achieves normal-incidence reflectance ranging from 35.1% at $\lambda = 28.1$ nm to 26.5% at $\lambda = 32.9$ nm. These reflectance values are considerably higher than those achieved with the traditional Si/Mo and Si/Mo_2C multilayers used in previous solar instruments (e.g., Si/Mo ranges from 22.4% to 15.5% over the same approximate wavelength range, and the reflectance of Si/Mo_2C is comparable), indicating that significant improvements in efficiency could be realized in future instruments utilizing this coating, in principle. For example, the efficiency of a two-reflection Cassegrain-type telescope tuned near 30 nm would more than double if it utilized Si/B_4C rather than Si/Mo coatings. As we discuss below, however, the adhesion of these Si/B_4C films is poor at present; until this critical problem can be solved these coatings are thus unsuitable for long-term use, as in a satellite instrument. The peak reflectance obtained with Si/C ranges from 19% to 16.9% over the range 27.5–32.3 nm; these values are smaller than the values of 20% at 28.3 nm and 25% at 30.4 nm for comparable Si/C films reported in Ref. 5, and the reason for this discrepancy is not known. The peak reflectances measured for Si/SiC multilayers are similar to those of Si/C, ranging from 18.5% to 16.7% over the same approximate range of wavelengths, though the spectral response of Si/SiC is much more narrow.

We can quantitatively characterize the spectral selectivity of multilayer coatings in a way that is particularly useful with regard to the design of solar imaging instruments by computing the effective rejection factor to adjacent wavelengths. We define this rejection factor as the peak reflectance at the target wavelength divided by the peak reflectance at the wavelength of the nearest bright solar emission line. We list rejection factors for each multilayer in the last column of Table 2; the rejection factors for coatings tuned to the Fe XV and Fe XVI lines refer to rejection of He II 30.4-nm radiation, while the rejection factor for He II multilayers refers to rejection of Fe XV emission at 28.4 nm. As can be seen from the table, the rejection factors for Si/B_4C exceed those of

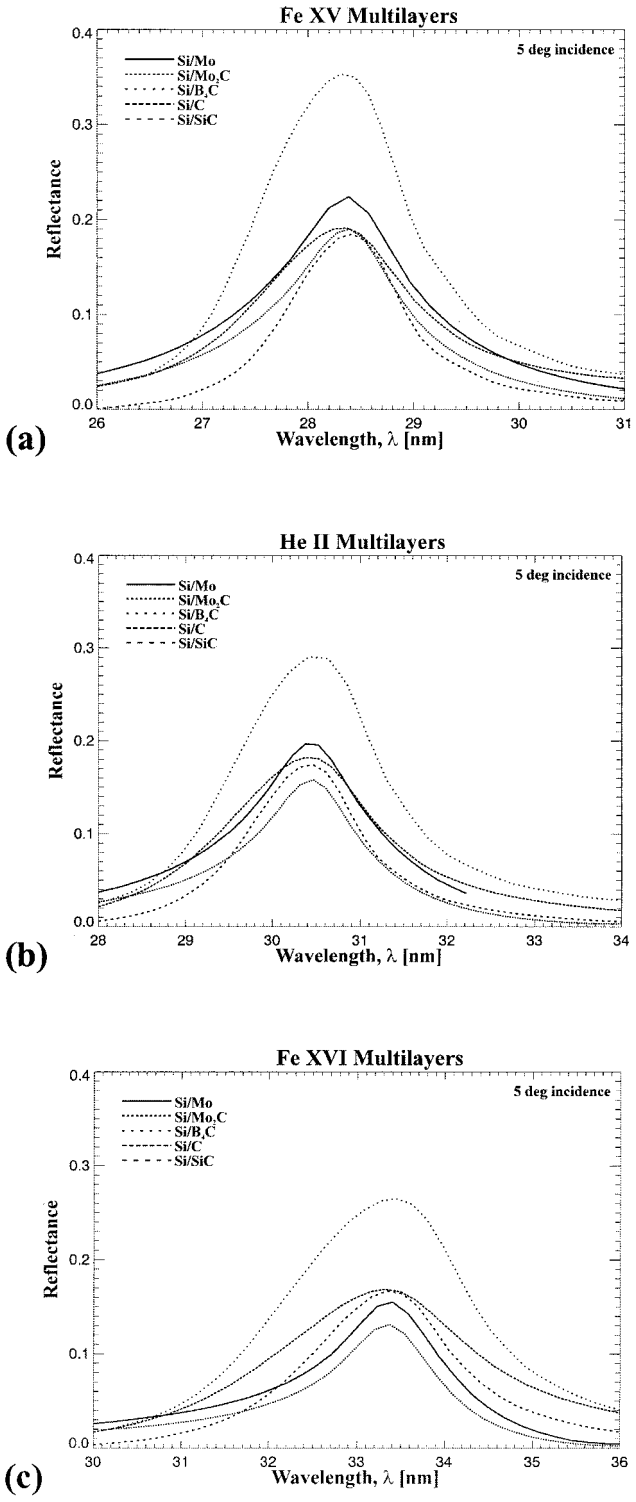

Fig. 1. Measured EUV reflectance of Si/Mo, Si/Mo_2C, Si/B_4C, Si/C, and Si/SiC multilayers tuned near (a) the solar Fe XV line at 28.4 nm, (b) the He II line at 30.4 nm, (c) the Fe XVI line at 33.5 nm. The structural parameters for each multilayer are listed in Table 2. The reflectance was measured at 5° incidence by use of synchrotron radiation at NSLS. The wavelength scale was adjusted slightly for each multilayer in these plots to compensate for small variations in multilayer period between samples, to facilitate relative performance comparisons.

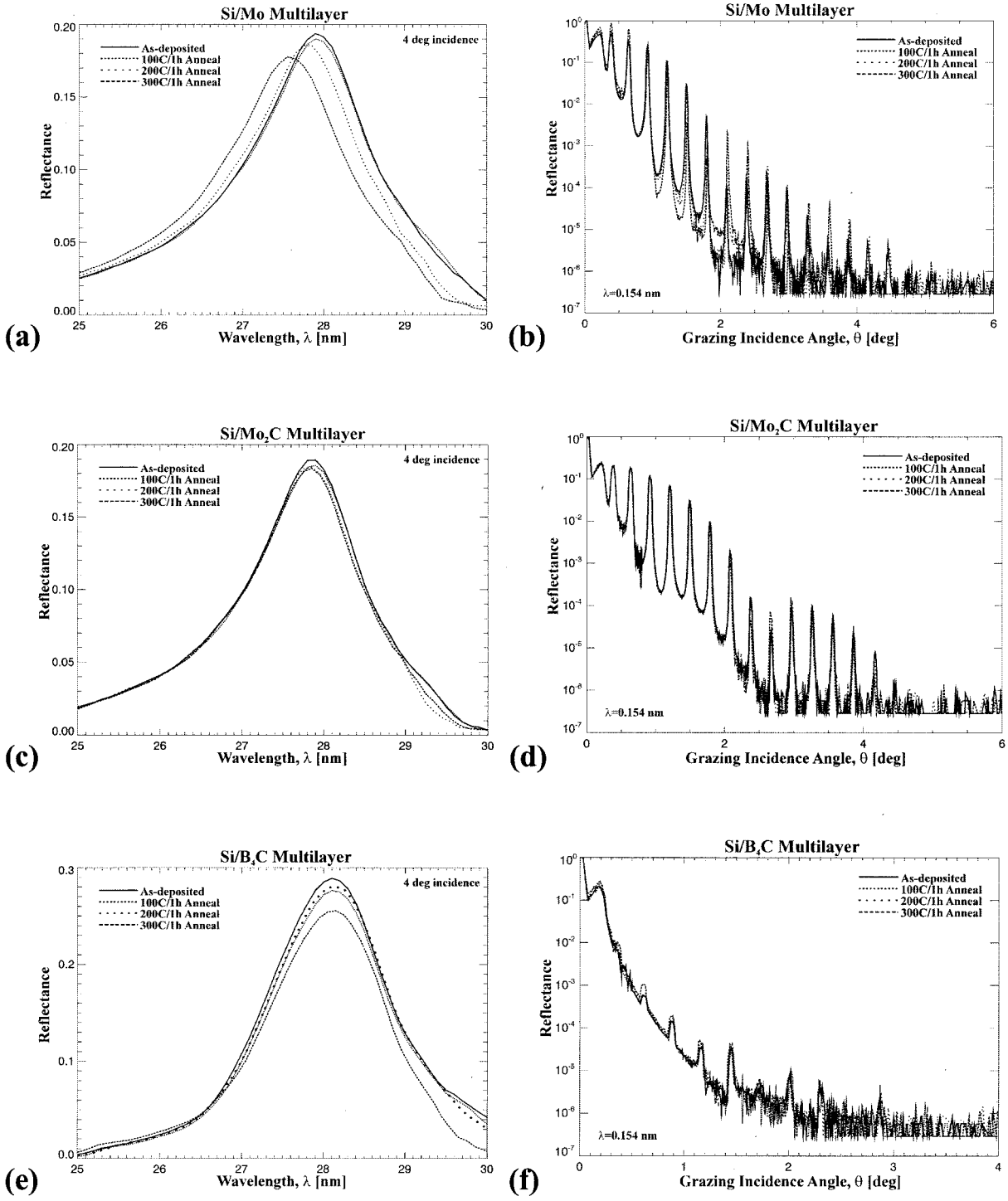

Fig. 2. Measured (a) normal-incidence EUV and (b) grazing-incidence x-ray reflectance of Si/Mo, (c), (d) Si/Mo_2C (e), (f) Si/B_4C (g), (h) Si/C, and (i), (j) Si/SiC multilayers, comparing the response for asdeposited films versus films annealed for 1 h at 100, 200, and 300 °C as indicated. The EUV reflectance measurements in this case were made at 4° incidence with a laser-plasma-based reflectometer (continues next page).

Si/Mo, Si/Mo_2C, and Si/C in all cases (even though the FWHM of Si/B_4C actually increases with wavelength); however, the highest spectral selectivity by far is obtained with Si/SiC multilayers: the rejection factor for Si/SiC ranges from 13.1×, for a coating tuned to 28.4 nm, to 15.0× for a coating tuned to 33.5 nm. In comparison, the rejection factors for Si/B_4C range from 7× to 10.3× over this same range, while the rejection factors for the other three multilayer systems are lower still. (Note that the rejection factors for a two-reflection telescope scale as the square of the numbers listed in Table 2.) Considering the

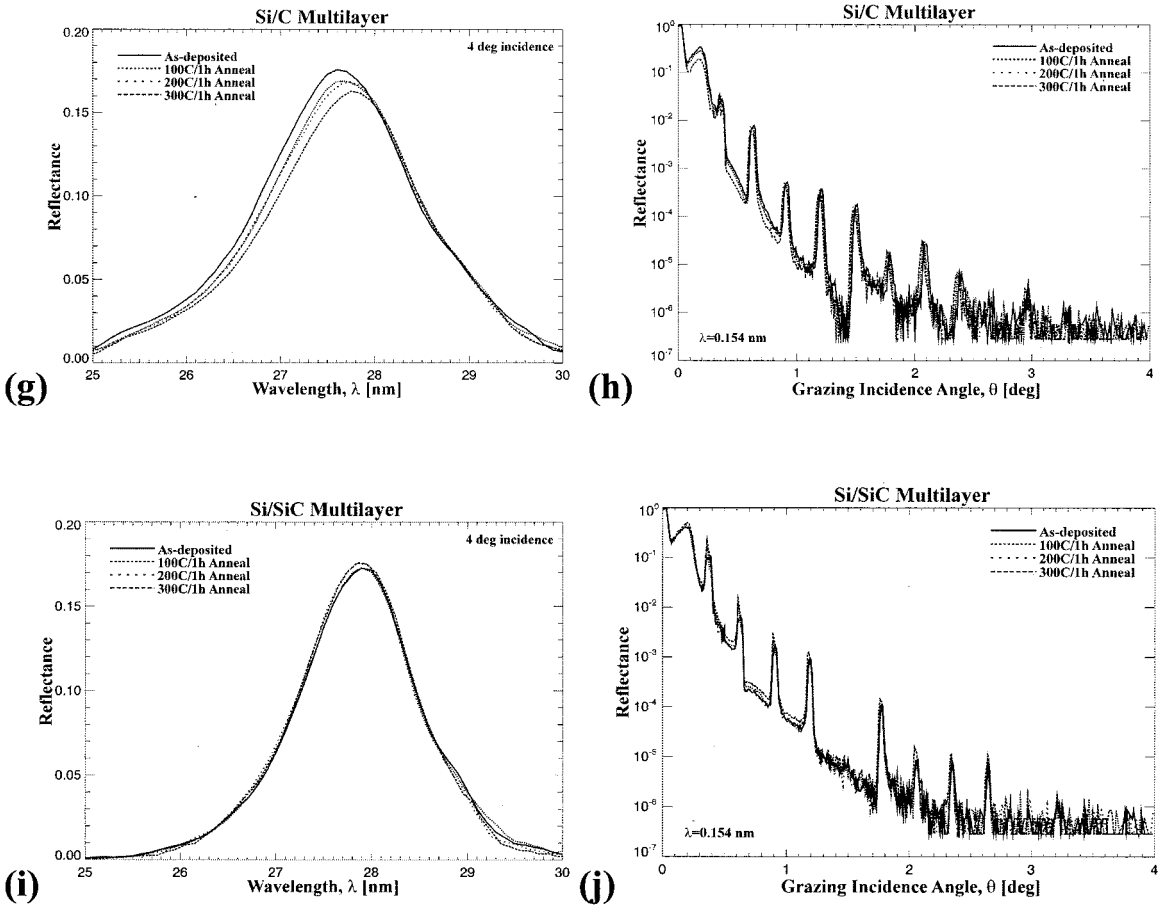

Fig. 2. (Continued).

relative intensity of the bright He II 30.4-nm line to the weaker Fe XVI 33.5-nm line, the greater spectral selectivity obtained with Si/SiC at the Fe XV and Fe XVI lines in particular, albeit with somewhat lower peak reflectance, may make this the preferred coating in many cases for these wavelengths. For example, assuming that the He II line is six times brighter than the Fe XVI line,[8] a two-reflection telescope tuned to the Fe XVI line would result in only ~2.7% spectral contamination by using Si/SiC coatings, but ~5.7% contamination by using Si/B_4C; the spectral contamination obtained by using any of the other coatings would be even greater, e.g., 22% contamination with Si/Mo. (The spectral selectivity of coatings tuned to the He II line is a far less important consideration, given the relative brightness of this line.)

The suitability of EUV multilayer coatings for use in space missions for solar physics depends not just on their EUV performance, but also on their long-term adhesion and their stability to heat, radiation, and energetic particles. The stability will become especially important with future missions such as the Solar Orbiter, whose planned orbit will take the spacecraft to within 45 solar radii (0.2 AU), thereby presenting an extreme environment to the constituent instruments.[16] We have assessed the thermal stability of the five multilayer systems just described by measuring the x-ray and EUV reflectance of each of these films before and after thermal anneals at 100, 200, and 300°C. The films were placed on a hotplate heated to the specified temperatures and were held for 1 h (in air) in order to promote any possible microstructural changes that might occur.

Shown in Fig. 2 are the measured EUV reflectance[17] and grazing-incidence XRR curves for the films tuned near the Fe XV line described above. With the notable exception of the Si/SiC film, all of the multilayers show some degradation in peak EUV reflectance and corresponding changes in the XRR data suggesting microstructural changes; the Si/Mo and Si/C films also show significant shifts in the peak wavelength, corresponding to a decrease or an increase, respectively, in the multilayer period. The decrease in peak reflectance observed in the Si/Mo_2C film is slight, as are the corresponding changes in the XRR data. In contrast to these four multilayer systems, the peak EUV reflectance of the Si/SiC film actually increases slightly (as do the heights of the XRR Bragg peaks) after thermal annealing.

A number of annealing-induced microstructural changes could explain the results shown in Fig. 2, including interfacial reaction, interfacial diffusion, compound formation, or any combination of these mechanisms. Without more detailed studies we

cannot untangle these effects and identify with certainty the precise explanation in each case. Nevertheless, we can conclude from the results presented here that all of these multilayers are reasonably stable when held to temperatures below 100 °C, which will quite likely be the maximum temperature experienced during any future solar mission as currently conceived. (The stability to radiation and energetic particles remains to be explored, however, as we discuss in Section 4.)

Adhesion problems, typically signified by crazing or delamination, have not been observed in any of the multilayers discussed here, with the notable exception of the Si/B_4C system: After approximately 10 months storage at room temperature in air, all of the Si/B_4C films began to craze. Presumably the poor adhesion in Si/B_4C is the result of high film stress (which has been observed in other B_4C-based multilayers); however, no quantitative stress measurements have been made on these films to date. We discuss in Section 4 below the prospects for solving this serious problem.

B. Broadband Multilayers for the Solar-B EIS

As described above, the imaging spectrometer comprising the Solar-B EIS instrument requires two different multilayer coatings, one tuned over the range $\lambda \sim 18$–21 nm, the other tuned for $\lambda \sim 25$–29 nm. These two wavelength bands include a number of bright lines from Fe X through Fe XXIV, as well as lines of He II, O V, Si VII, Si X, and Ca XVII. To maximize the scientific return from this instrument (currently planned for launch in 2006), the response of the multilayers must be optimized for both high reflectance and broad spectral response.

Si/Mo multilayers were identified for use in the baseline EIS instrument design; however we also considered the use of Si/Mo_2C multilayers, given the good results obtained previously with the TRACE instrument. As in the case of the narrowband multilayers discussed above, modeling again suggested that better performance could be achieved for the long-band EIS coatings by using multilayers having Mo or Mo_2C as the topmost layers. In order to mitigate oxidation of the metal layers, 2-nm-thick Si protective capping layers were used. We determined the effectiveness of the capping layers by measuring the EUV reflectance of capped versus uncapped Si/Mo and Si/Mo_2C multilayers before, during, and after long-term thermal annealing at 80°C in air. Similar to the thermal annealing work described above, samples were placed on a hotplate in (humid, East-coast summer) air; in this case, however, we examined the reflectance after 3 and 8 days of annealing. The lower temperatures and longer annealing times are intended to promote surface oxidation rather than structural changes within the multilayer stack. Results obtained with prototype long-band EIS multilayers are shown in Fig. 3: The uncapped multilayers show large reductions in reflectance over time, whereas the capped multilayers show only slight reductions in reflectance. Modeling (outlined below) indicates that the relatively small changes in the capped multilayers are fully consistent with oxidation of the Si capping layers. The observed shifts (toward longer wavelengths) in the peak wavelengths in this case are due to refraction in the surface oxide and are not associated with any changes in the multilayer period (verified from XRR measurements), in contrast to the peak shifts (towards shorter wavelengths) observed in the Si/Mo films annealed at higher temperatures discussed above [Figs. 2(a) and 2(b)]. Once the capping layers oxidize, the resulting SiO_2 layer is known to be relatively stable and resistant to further changes resulting from exposure to air, suggesting that the capped metal-on-top multilayers are an acceptable choice for the EIS instrument.

In the case of the Si/Mo_2C films, we also discovered a sensitive dependence of EUV reflectance and interface width σ on the background pressure in the coating chamber before deposition. Shown in Fig. 4(a) are the EUV reflectance measurements, and in Fig. 4(b) the XRR data, for two otherwise identical Si/Mo_2C multilayers having $N = 20$ bilayers, period $d = 14.72$ nm, and $\Gamma = 0.7$; but, by varying the pumping time in the vacuum chamber prior to deposition, one sample was prepared at a background pressure of 5.0×10^{-6} Torr, the other at 7.6×10^{-7} Torr. The peak EUV reflectance for the low-pressure sample is 19.8%, while that of the high-pressure sample is 17.4%; the average interface widths determined from fits to the XRR data [Fig. 4(b)] show a corresponding increase from 0.48 to 0.65 nm for these samples as well.

A similar dependence of interface width on background pressure was observed previously in the case of Si/W multilayers designed for use as hard-x-ray reflective coatings.[18] In addition, a sensitive dependence of film stress on background pressure was observed in Si/Mo EUV multilayers,[19] although in that study no variations in the EUV reflectance were observed, a result reconfirmed in the present work. In that latter study (Ref. 19), the variation in stress was associated with an increase in atomic H incorporated into the film, as determined from forward recoil scattering measurements; it was suggested that water vapor (the predominant residual gas present in the coating chamber mentioned above used in all these studies) may condense on the surface of the growing film and act to reduce the effective surface mobility of adatoms, thereby increasing the interfacial roughness in these multilayers through self-shadowing.[20] This mechanism could also be responsible for the behavior observed in Si/Mo_2C multilayers; lower intrinsic surface mobility of Mo_2C adatoms relative to Mo, B_4C, C, and SiC adatoms would explain why no comparable increase in interfacial roughness was observed in Si/Mo, Si/B_4C, Si/C, or Si/SiC multilayers.

Whatever the explanation, as a consequence of the results shown in Fig. 4, and although we ob-

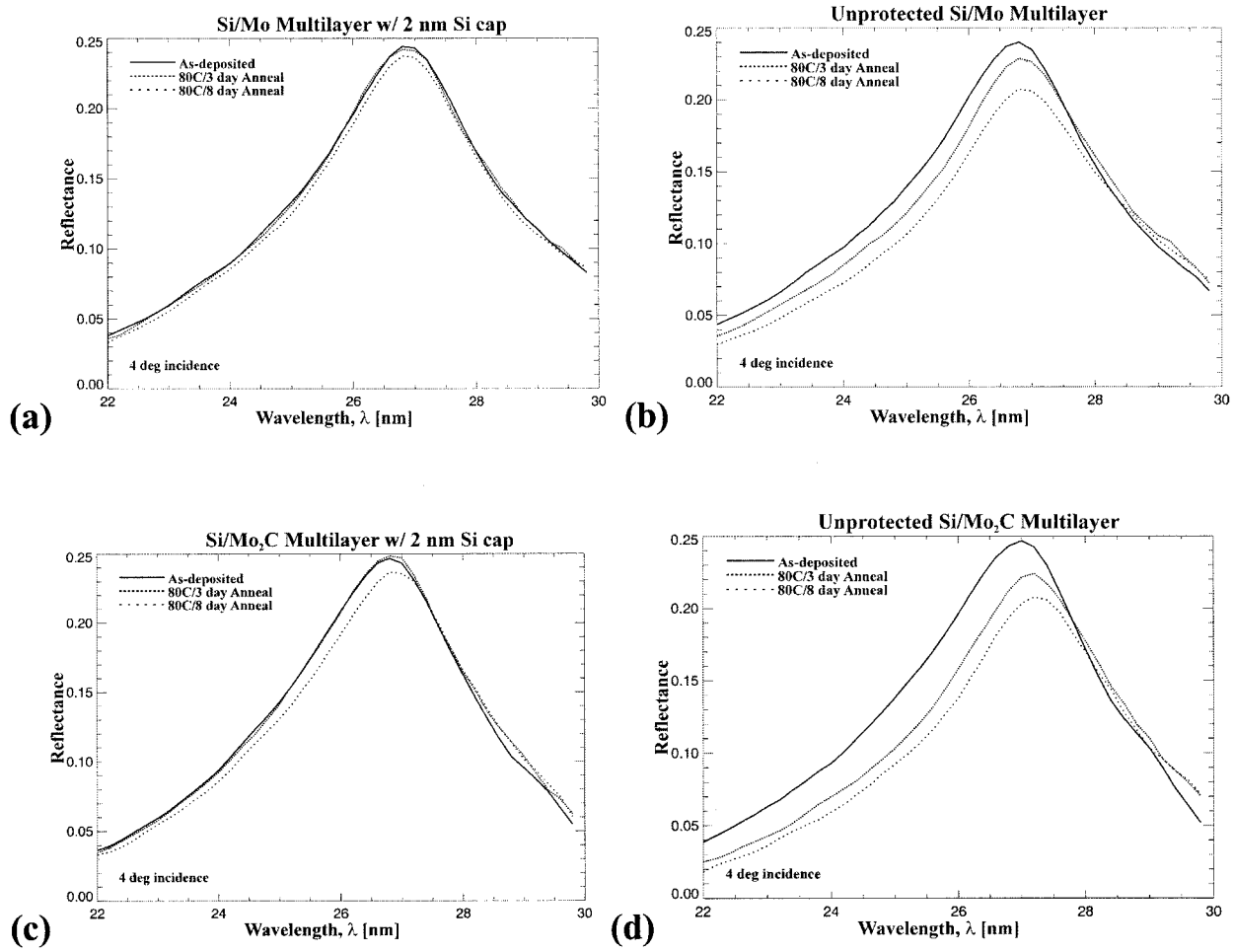

Fig. 3. Measured EUV reflectance Si/Mo and Si/Mo_2C multilayers, comparing as-deposited films with those annealed at 80°C in air for 3 days and 8 days, as indicated. All four films have metal (i.e., Mo or Mo_2C) as the topmost layer; the Si/Mo film in (a) and the Si/Mo_2C film in (c) have 2-nm-thick Si capping layers, and the films in (b) and (d) are unprotected.

served no similar dependence of EUV reflectance on background pressure in any of the other multilayer systems discussed here, all other multilayer samples described here were prepared at a background pressure of less than 10^{-6} Torr, as already noted above.

Shown in Figs. 5(a) and 5(b) are the measured EUV reflectance-versus-wavelength curves for two series

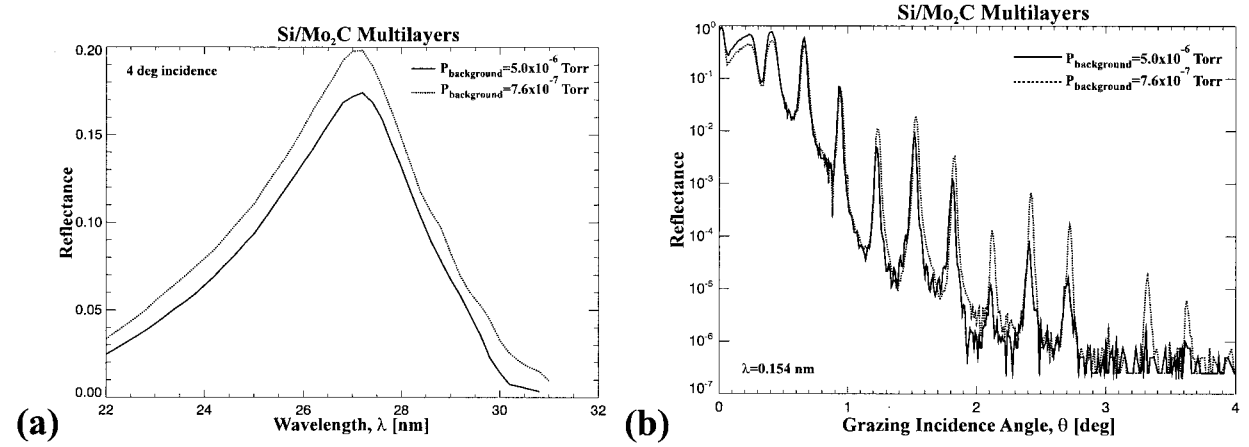

Fig. 4. Measured (a) normal-incidence EUV and (b) grazing incidence x-ray reflectance of Si/Mo_2C multilayers prepared at high versus low background pressure as indicated.

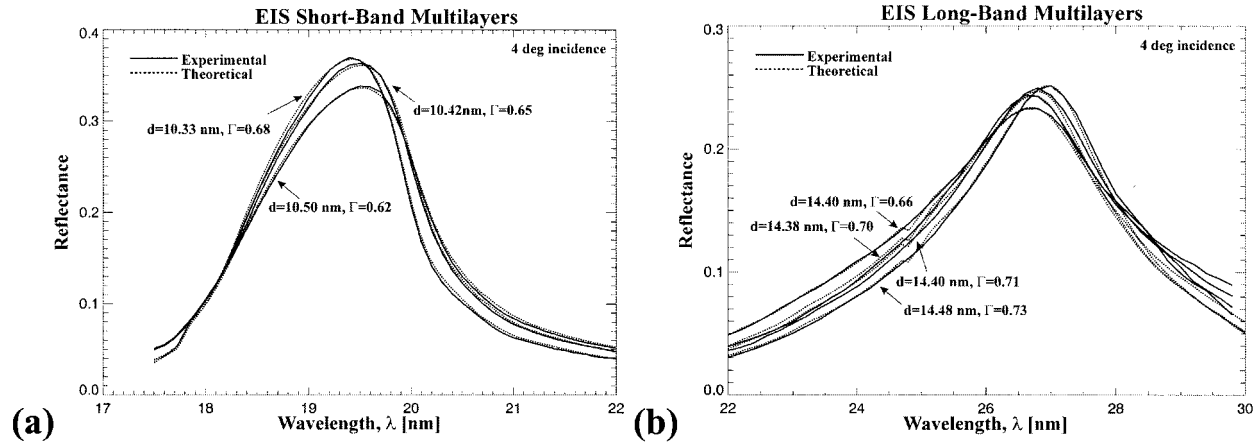

Fig. 5. Comparison of the measured EUV reflectance of prototype multilayers for the Solar-B EIS instrument, demonstrating how the spectral response of the coatings can be fine-tuned by precisely adjusting individual Si and Mo layer thicknesses as indicated. Fits to the measured curves (with the optical constants for Si from Ref. 21 and for Mo from Ref. 22) are shown as dotted curves.

of prototype Si/Mo multilayer coatings for the EIS short- and long-band instrument channels, containing $N = 20$ bilayers, and having periods of order 10.4 and 14.4 nm, respectively. The fractional Si-layer-thicknesses Gamma for the films shown in Fig. 5(a) range from 0.62 to 0.68, while those in Fig. 5(b) range from 0.66 to 0.73; these results illustrate how the spectral response of the coatings can be fine-tuned by precisely varying the individual Si and Mo layer thicknesses. The measured multilayer curves shown in Fig. 5 were used to model the full EIS instrument response function, and on the basis of these results, in consideration of the anticipated solar emission, in the end the EIS optics were coated with Si/Mo films having $d = 10.42$ nm, $\Gamma = 0.65$ for the short-band channel, and $d = 14.4$ nm, $\Gamma = 0.66$ for the long-band channel. The details regarding the coating of the flight optics, including instrument calibration and techniques used to control the coating thickness uniformity, will be not be presented here.

C. EUV Reflectance Modeling and Optical Constants

The ability to model accurately and precisely the response of EUV multilayer structures is important for the development of new multilayer instrument designs, for the generation of reliable instrument response functions once an instrument has been developed and calibrated, and for understanding the fundamental relationships between film structure and optical performance in emerging as well as in mature multilayer systems. The reflectance of the multilayers discussed above was modeled with IMD, which uses an algorithm based on recursive application of the Fresnel equations (modified to account for interface imperfections) to describe the reflectance and transmittance at each interface in the multilayer stack. The accuracy and validity of this approach, and of the structural parameters derived from the fits, depends crucially on the accuracy of the optical constants used in the calculation, on detailed knowledge of the layer and interface morphology, and on the condition of the surface (especially in the EUV where thin surface contamination layers can strongly affect the normal-incidence reflectance.) At the EUV wavelengths considered here, unfortunately, the availability of accurate optical constants remains poor, in general, in spite of continuing efforts to measure these quantities for technologically important materials. The lack of reliable optical constants, coupled with the presence of unknown surface contamination layers and, in certain multilayers, interfacial layers of mixed composition (e.g., the amorphous Si–Mo interlayers observed in Si/Mo multilayers) whose precise optical constants are not known at EUV wavelengths makes accurate modeling difficult if not impossible in many cases.

Shown in Fig. 6(a) is the measured normal-incidence reflectance of a broadband Si/Mo multilayer tuned near $\lambda \sim 27$ nm. The dashed curve is the best fit that could be achieved by using optical constants for Si and Mo determined from the atomic scattering factors available from the Center for X-Ray Optics (CXRO);[21] clearly this fit does not agree very well with the measured response of the coating. Fortunately, new optical constants for Mo (as well as for C and B_4C,) were determined recently by reflectance-versus-incidence angle measurements made *in situ* for films deposited under ultrahigh-vacuum conditions.[22] The fit obtained by using these optical constants for Mo, along with the CXRO data for Si, are shown as the dotted curve in Fig. 6(a); the agreement with the measured reflectance is markedly improved. For this fit we infer an interface width of 1.3 nm for the Si-on-Mo interfaces and 0.3 nm for the Mo-on-Si interfaces. Comparably good fits to the EIS prototype coatings with these optical constants are shown as dotted curves in Fig. 5 as well.

In contrast, shown in Fig. 6b is the measured reflectance of a narrowband Si/Mo multilayer tuned to a slightly longer wavelength; even by using the Mo optical constants from Ref. 22, the best fit to the data

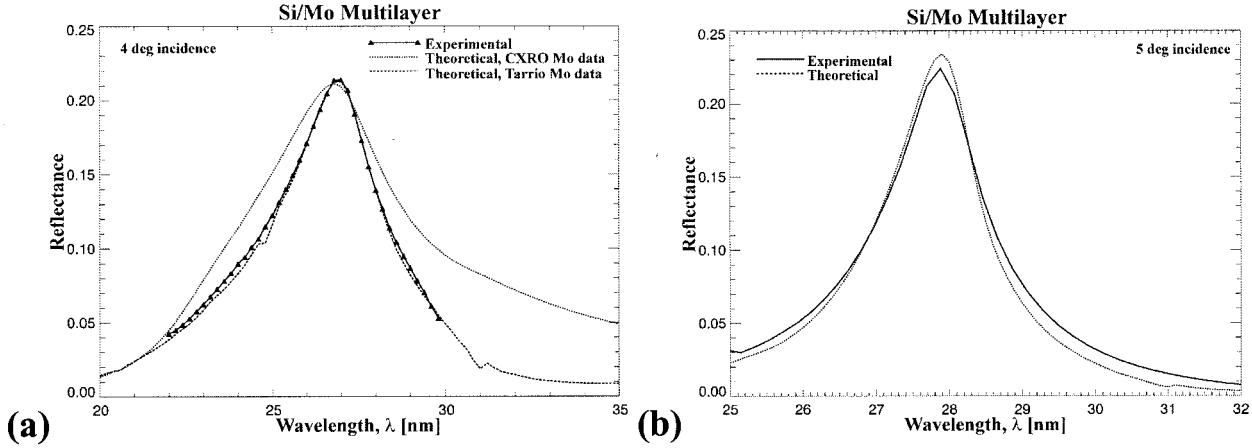

Fig. 6. Measured EUV reflectance of broadband (a) and narrowband (b) Si/Mo multilayers. The dotted curve in (a) is a fit to the data using the CXRO optical constants from Ref. 21 for Si and Mo; dashed line is fit using the optical constants for Mo from Ref. 22; and is markedly better. The quality of the fit (dotted curve) for the narrowband multilayer (b) using the Tarrio data for Mo is poor, however.

is far from perfect. (Note that all the fits discussed here for films containing 2.0-nm-thick Si capping layers were modeled by using 1.5-nm-thick amorphous SiO_2 on 1.0-nm Si in order to account for the oxidation of the Si capping layer.) Furthermore, the structural parameters determined from this fit, i.e., d, Γ, and σ, differ significantly from those parameters determined from XRR measurements. This discrepancy is apparent in Table 2, for Si/Mo, as well as all the other multilayer systems shown here. (Because good-quality fits could not be achieved for the narrowband multilayers listed in Table 2 by using asymmetric interface widths, as in Fig. 6(a), for simplicity we list the average σ values inferred from models assuming symmetric interfaces.) In the case of the narrowband Si/Mo films, the discrepancy may be due to the presence of the amorphous Si–Mo interlayers mentioned above: in these high-Γ multilayers the interlayer widths account for a greater fraction of the total bilayer thickness, and so the modified Fresnel coefficient formalism used to account for these interface imperfections (which is essentially a Born approximation that assumes small perturbations) may no longer be valid.

Shown in Fig. 7 are the measured reflectance curves of two Si/Mo_2C multilayers, along with fits made by using the CXRO optical constants for Si and Mo_2C (dotted curves). Also shown are fits made with newly derived optical constants for Mo_2C (dashed curves). These new Mo_2C optical constants, shown in Fig. 8, were determined for a sputtered Mo_2C film prepared in the deposition system mentioned above by fitting reflectance-versus-incidence angle measurements[23] made by using the Columbia reflectometer; even with the known systematic errors in these reflectance measurements, as described above, the fit to the broadband multilayer curve in Fig. 7(a) is significantly better than the fit made by

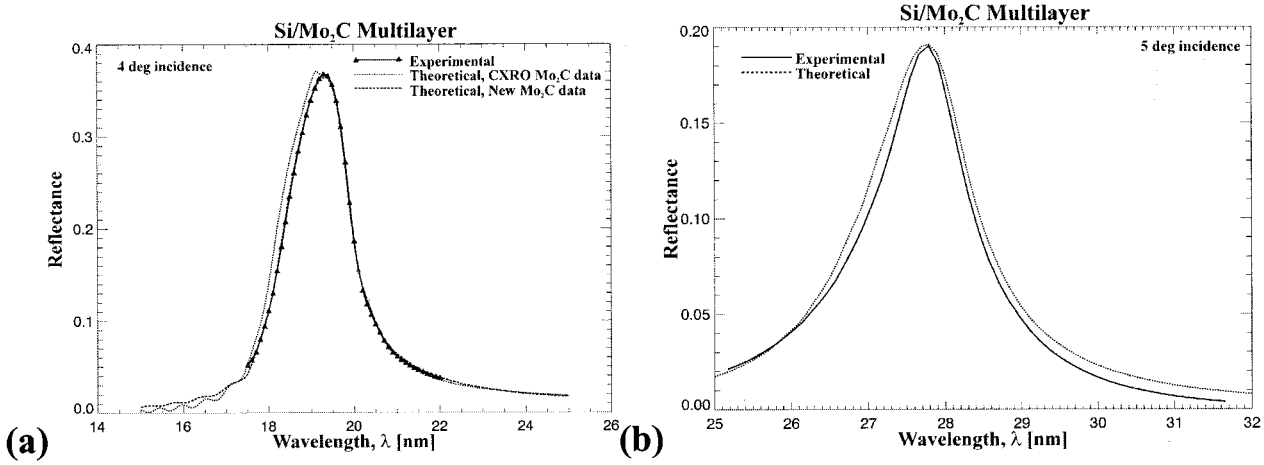

Fig. 7. Measured EUV reflectance of (a) broadband (a) and (b) narrowband Si/Mo_2C multilayers. The dotted curve in (a) is a fit to the data using the CXRO optical constants from Ref. 21 for Si and Mo_2C; the dashed curve is fit using newly derived optical constants for Mo_2C shown in Fig. 8 and is markedly better. The quality of the fit (dotted line) for the narrowband multilayer (b) using the new data for Mo_2C is poor, however.

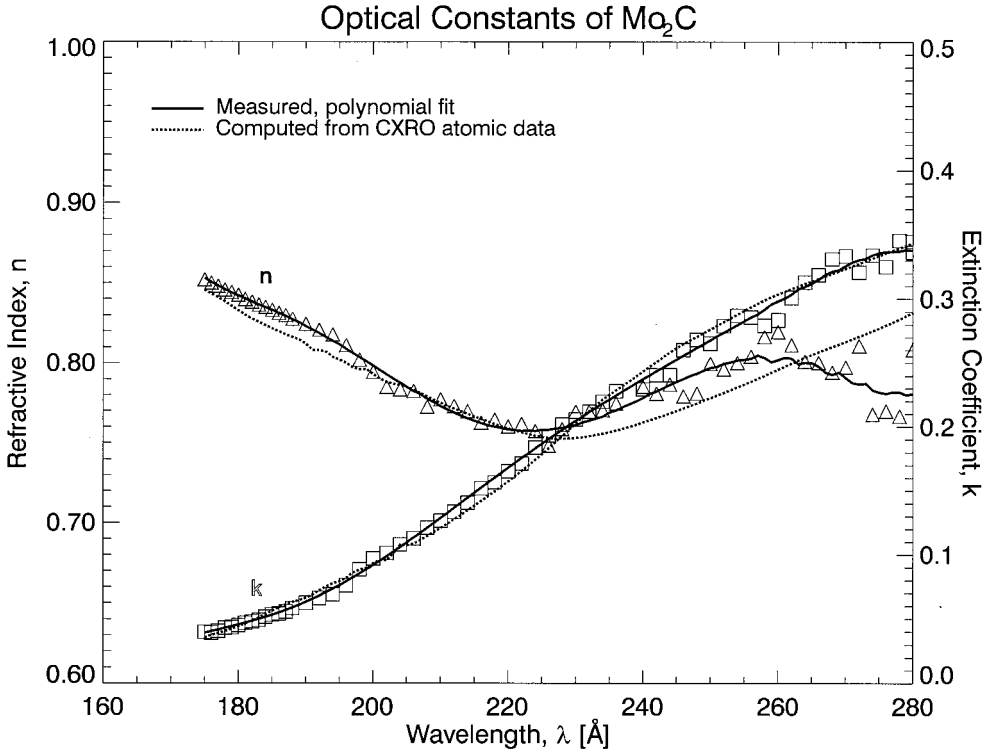

Fig. 8. Optical constants (refractive index, n, and extinction coefficient, k) for Mo_2C, determined by fitting reflectance versus incidence angle measurements of a sputtered Mo_2C film. The solid curves are polynomial fits to the measured data. The optical constants determined from the CXRO atomic scattering factors[21] are shown as dotted curves.

using the CXRO optical constants. However, as in the case of the Si/Mo films shown in Fig. 6(b), the best fit to the high-Γ, narrowband multilayer [Fig. 7(b)] is relatively poor, and the discrepancy between the EUV and XRR structural parameters listed in Table 2 is again large. The cause of the discrepancy in this case is not known, though it might be due to the presence of interfacial layers, as in the Si/Mo film discussed above.

Example fits to selected narrowband Si/B_4C, Si/C, and Si/SiC multilayers are shown in Fig. 9. The calculated reflectance curves shown in this figure were made by using the CXRO data for Si and SiC and the data from Ref. 22 for C and B_4C. Once again these fits are imperfect, especially for the Si/B_4C and Si/C films, and large discrepancies remain between the XRR and EUV structural parameters for all three multilayers systems listed in Table 2.

4. Conclusions

We have described our research results directed at the development of optimized EUV multilayers for future narrowband solar imagers. We have made a systematic comparison of multilayers comprising Si/Mo, Si/Mo_2C, Si/B_4C, Si/C, and Si/SiC bilayers, all designed for narrowband imaging in the wavelength range $\lambda \sim 25$–35 nm. This portion of the EUV is of particular interest for the development of future solar imagers.

We find that the highest reflectance in this wavelength range can be realized with Si/B_4C multilayers. Unfortunately, however, and in spite of relatively good thermal stability, the adhesion of Si/B_4C multilayers was found to be poor, with crazing observed in all the films studied here after approximately 10 months storage in air. The poor adhesion is likely due to high film stress; assuming for the moment that stress is indeed the cause, then we can hope to reduce the film stress and thus improve the adhesion in the future through control of the deposition process. For example, it may be possible to reduce the film stress sufficiently without degrading the EUV reflectance simply by increasing the Ar sputter gas pressure during film growth, a technique that has been successfully exploited previously in order to produce low-stress W/Cr bilayers, for example.[24] In any case, and whatever the cause, until the adhesion problem is solved, Si/B_4C coatings cannot be considered suitable at present for long-term use, as in a space mission.

With regard to spectral selectivity, we find among the multilayers discussed here that the best performance is obtained with the newly developed Si/SiC multilayer system: for example, assuming that the He II 30.4-nm line is six times brighter than the nearby Fe XVI 33.5-nm line, a two-reflection telescope tuned to the Fe XVI line would result in only ~2.7% spectral contamination by using Si/SiC coatings, while an equivalent telescope coated with Si/Mo would yield 22% contamination.

From thermal annealing experiments we have found that the thermal stability of all of the multi-

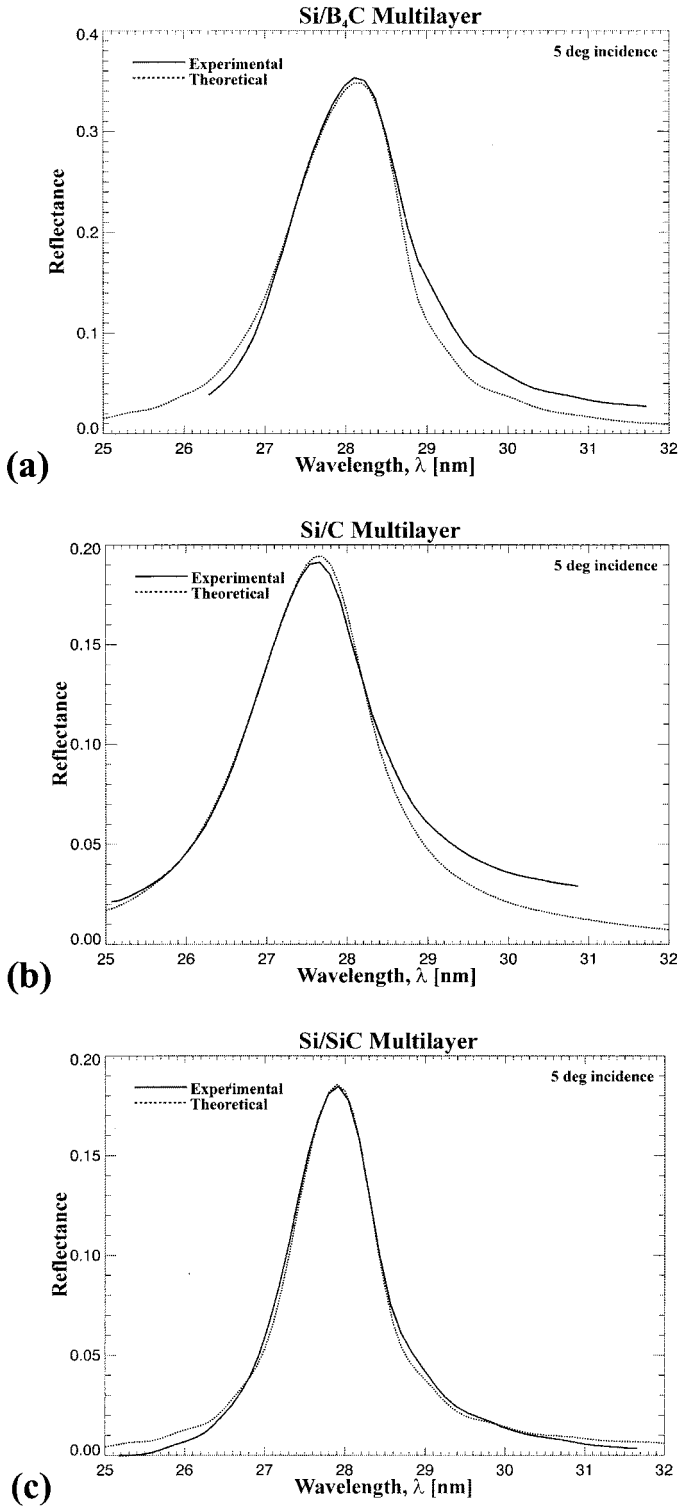

Fig. 9. EUV reflectance of (a) Si/B_4C, (b) Si/C, and (c) Si/SiC multilayers. The measured values are shown as solid curves while the dotted curves are fits using optical constants for Si and SiC from Ref. 21 and for B_4C and C from Ref. 22.

layers discussed here is adequate for use in space-based missions provided that the instrument temperature is held below 100 °C, excluding, of course, the Si/B_4C system, in light of the adhesion problem discussed above. However the stability to intense solar radiation, and to intense bombardment by energetic particles (i.e., MeV protons), as expected for certain missions such as the planned Solar Orbiter, is unknown and is clearly a beckoning topic for future research.

We have also described research directed at the optimization of Si/Mo and Si/Mo_2C multilayers hav-

ing broad spectral response, as required, for example, for the Solar-B EIS instrument currently under development. We have described how the spectral response of these coatings can be fine-tuned by adjusting the fractional metal-layer thickness and have demonstrated that high reflectance can be obtained with films that have Mo or Mo_2C as the topmost layer in the multilayer stack, in conjunction with 2-nm-thick Si capping layers used to effectively mitigate oxidation of the underlying metal layer.

Finally, by comparing XRR and EUV reflectance measurements, we find that our ability to accurately model the EUV performance of these multilayers remains imperfect, in general, as does our ability to reconcile structural parameters determined from these two complementary characterization techniques. Much of this trouble can be ascribed to inaccurate or incomplete optical constants in the EUV (another area that would benefit greatly from further research) and to imperfect knowledge of the detailed interface and surface structure in these films.

The authors acknowledge a number of individuals and groups for their important contributions to this research: E. Gullikson (ALS) for assisting with cross-calibration measurements between the ALS, NSLS and Columbia reflectometers; C. Tarrio (National Institute of Standards and Technology) for providing his tabulated optical constants; C. Brown, K. Dere, G. Doschek, C. Korendyke, J. Mariska, S. Myers, and the entire Naval Research Laboratory Solar-B EIS team for their financial support as well as important contributions regarding the EIS multilayer requirements; L. Harra and J. L. Culhane (Mullard Space Science Laboratory) for important discussions regarding the stability of EUV multilayers for the Solar Orbiter; and L. Golub, E. Deluca, J. Bookbinder (Smithsonian Astrophysical Observatory), and D. McKenzie (Montana State University) for important discussions regarding EUV multilayer response requirements for future solar imaging missions.

This research was sponsored in part by a grant from NASA.

References and Notes

1. D. G. Stearns, M. B. Stearns, Y. Cheng, J. H. Stith, and N. M. Ceglio, "Thermally induced structural modification of Mo–Si multilayers," J. App. Phys. **67,** 2415–2427 (1990).
2. J. M. Slaughter, A. Shapiro, P. A. Kearney, and C. M. Falco, "Growth of molybdenum on silicon: structure and interface formation," Phys. Rev. B **44,** 3854–3763 (1991).
3. D. L. Windt, R. Hull, and W. K. Waskiewicz, "Interface imperfections in metal/Si multilayers," J. Appl. Phys. **71,** 2675–2678 (1992).
4. J. M. Slaughter, B. S. Medower, R. N. Watts, C. Tarrio, T. B. Lucatorto, and C. M. Falco, "Si/B_4C narrow-bandpass mirrors for the extreme ultraviolet," Opt. Lett. **19,** 1786–1788 (1994).
5. M. Grigonis and E. J. Knystautas, "C/Si multilayer mirrors for the 25–30 nm wavelength region," Appl. Opt. **36,** 2839–2842 (1997).
6. M. Malinovsky and L. Heroux, "An analysis of the solar extreme-ultraviolet spectrum between 50 and 300 Å," Astrophys. J. **181,** 1009–1030 (1973).
7. G. A. Doschek and R. D. Cowan, "A solar spectral line list between 10 and 200 Å modified for application to high spectral resolution x-ray astronomy," Astrophys. J. Suppl. **56,** 67–89 (1984).
8. R. J. Thomas and W. M. Neupert, "Extreme ultraviolet spectrum of a solar active region from SERTS," Astrophys. J. Suppl. **91,** 461–482 (1994).
9. J. P. Delaboudinière, G. E. Artzner, J. Brunaud, A. H. Gabriel, J. F. Hochdez, F. Millier, X. Y. Song, B. Au, K. P. Dere, R. A. Howard, R. Kreplin, D. J. Michels, J. D. Moses, J. M. Defise, C. Jamar, P. Rochus, J. P. Chauvineau, J. P. Marioge, R. C. Catura, J. R. Lemen, L. Shing, R. A. Stern, J. B. Gurman, W. M. Neupert, A. Maucherat, F. Clette, P. Cugnon, and E. L. Van Dessel, "EIT: extreme-ultraviolet imaging telescope for the SOHO mission," Solar Phys. **162,** 291–312 (1995).
10. B. N. Handy, L. W. Acton, C. C. Kankelborg, C. J. Wolfson, D. J. Akin, M. E. Bruner, R. Caravalho, R. C. Catura, R. Chevalier, D. W. Duncan, C. G. Edwards, C. N. Feinstein, S. L. Freeland, F. M. Friedlander, C. H. Hoffmann, N. E. Hurlburt, B. K. Jurcevich, N. L. Katz, G. A. Kelly, J. R. Lemen, M. Levay, R. W. Lindgren, D. P. Mathur, S. B. Meyer, S. J. Morrison, M. D. Morrison, R. W. Nightingale, T. P. Pope, R. A. Rehse, C. J. Schrijver, R. A. Shine, L. Shing, T. D. Tarbell, A. M. Title, D. D. Torgerson, L. Golub, J. A. Bookbinder, D. Caldwell, P. N. Cheimets, W. N. Davis, E. E. DeLuca, R. A. McMullen, D. Amato, R. Fisher, H. Maldonado, and C. Parkinson, "The transition region and coronal explorer," Solar Phys. **187,** 229–260 (1999).
11. L. Golub and J. M. Pasachoff, *The Solar Corona* (Cambridge U. Press, Cambridge, UK, 1997), chap. 8.
12. J. Seely, "Multilayer grating for the extreme ultraviolet spectrometer (EIS)," in *X-Ray Optics, Instruments, and Missions IV*, R. B. Hoover and A. B. Walker II, eds., Proc. SPIE **4138,** 174–181 (2002).
13. D. L. Windt and W. K. Waskiewicz, "Multilayer facilities required for extreme-ultraviolet lithography," J. Vac. Sci. Technol. B **12,** 3826–3832 (1994).
14. D. L. Windt, "IMD — software for modeling the optical properties of multilayer films" Comput. Phys. **12,** 360–370 (1998).
15. J. H. Underwood, E. M. Gullikson, M. Koike, P. J. Batson, P. E. Denham, K. D. Franck, R. E. Tackaberry, and W. F. Steele, "Calibration and standards beamline 6.3.2 at the Advanced Light Source," Rev. Sci. Inst. **67,** 3372 (1996).
16. Solar Orbiter Pre-Assessment Study Report, October 1999, http://zeus.nascom.nasa.gov/~bfleck/Orbiter/Documents/pre_assess_rep.pdf.
17. These EUV reflectance data were obtained by use of the laser-plasma-based reflectometer described above; in this case no adjustments to the wavelength scales were made.
18. D. L. Windt, F. E. Christensen, W. W. Craig, C. Hailey, F. A. Harrison, M. Jimenez-Garate, R. Kalyanaraman, and P. H. Mao, "Growth, structure and performance of depth-graded W/Si multilayers for hard X-ray optics," J. Appl. Phys. **88,** 460–470 (2000).
19. D. L. Windt, W. L. Brown, C. A. Volkert, and W. K. Waskiewicz, "Variation in stress with background pressure in sputtered Mo/Si multilayer films," J. Appl. Phys. **78,** 2423–2430 (1995).
20. J. Dalla Torre, G. H. Gilmer, D. L. Windt, R. Kalyanaraman, F. H. Bauman, P. L. O'Sullivan, J. Sapjeta, T. Diaz de la Rubia, and M. Djafari Rouhani, "Microstructure of thin tantalum films sputtered onto inclined substrates: experiments and atomistic simulations," J. App. Phys. **94,** 263–271 (2003).
21. B. L. Henke, E. M. Gullikson, and J. C. Davis, "X-ray interactions: photabsorption, scattering, transmission, and reflection at $E = 50$–$30{,}000$ eV, $Z = 1$–92," At. Data Nuclear Data Tables **54,** 181–342 (1993).

22. C. Tarrio, R. N. Watts, T. B. Lucatorto, J. M. Slaughter, and C. M. Falco, "Optical constants of *in situ* deposited films of important extreme-ultraviolet multilayer mirror materials," App. Opt. **37,** 4100–4104 (1998).
23. D. L. Windt, W. Cash, M. Scott, P. Arendt, B. Newnam, R. F. Fisher, A. B. Swartzlander, M. Pinneo, and P. Z. Takacs, "Optical constants for thin films of C, diamond, Al, Si, and CVD-SiC from 24 Å to 1216 Å," Appl. Opt. **27,** 279–295 (1988).
24. D. L. Windt, "Low-stress W/Cr bilayer films for use as SCALPEL® mask scattering layers," J. Vac. Sci. Tech. B **17,** 1385–1389 (1999).